

# Spacetime Markov length: a diagnostic for fault tolerance via mixed-state phases

Amir-Reza Negari<sup>1,2,\*</sup>, Tyler D. Ellison<sup>1</sup>, and Timothy H. Hsieh<sup>1,2</sup>

<sup>1</sup>*Perimeter Institute for Theoretical Physics, Waterloo, Ontario N2L 2Y5, Canada and*

<sup>2</sup>*Department of Physics and Astronomy, University of Waterloo, Waterloo, Ontario N2L 3G1, Canada*

We establish a correspondence between the fault-tolerance of local stabilizer codes experiencing measurement and physical errors and the mixed-state phases of decohered resource states in one higher dimension. Drawing from recent developments in mixed-state phases of matter, this motivates a diagnostic of fault-tolerance, which we refer to as the spacetime Markov length. This is a length scale determined by the decay of the (classical) conditional mutual information of repeated syndrome measurement outcomes in spacetime. The diagnostic is independent of the decoder, and its divergence signals the intrinsic breakdown of fault tolerance. As a byproduct, we find that decoherence may be useful for exposing transitions from higher-form symmetry-protected topological phases driven by both incoherent and coherent perturbations.

**Introduction:** The threshold theorem [1–4] is a cornerstone of quantum fault tolerance, ensuring that quantum computations can be reliably performed if error rates are below a certain threshold. It is well known that the error threshold, in certain cases, can be related to an order-to-disorder phase transition by mapping the decoding problem to a classical statistical-mechanics model [5–7]. However, given the inherent competition between decoherence and error correction, it is natural to wonder whether the threshold can be viewed instead as a transition at the level of quantum states—between distinct mixed-state phases of matter. There has been significant recent progress in understanding mixed-state phases of matter [8–42], so such a connection would allow for renewed perspectives on quantum error correction enabled by our developing understanding of quantum phases of matter.

A fundamental component of fault tolerance is quantum error correction, which often requires repeating error syndrome measurements to compensate for the fact that the measurements themselves may be faulty. In the idealistic case of perfect measurements, there has been remarkable progress in relating noisy error-correcting codes to mixed-state entanglement properties and mixed-state phases of matter [12–16]. The paradigmatic example of this is the toric code subjected to local Pauli noise, in which the breakdown of the quantum memory can be understood as a mixed-state phase transition induced by the noise. Note that, in this context, a mixed-state phase is taken to be an equivalence class of states, where two states are considered to be in the same mixed-state phase if there exist local Lindbladian evolutions that transform one into the other [11].

Despite this progress, such a relation for the fully fault-tolerant setting, which includes repeated faulty measurements, has yet to be established. This necessitates taking a spacetime perspective on fault tolerance, in which physical and measurement errors appear at locations throughout spacetime [43]. This perspective is

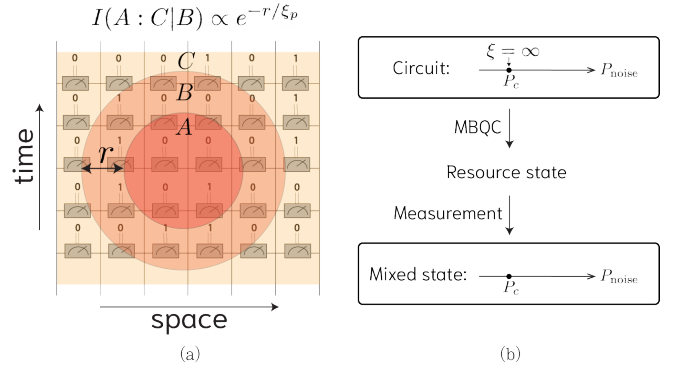


FIG. 1. (a) A schematic of computing the CMI of a circuit with repeated syndrome measurements. The ensemble of measurement outcomes in spacetime is tri-partitioned, and its CMI is given by  $I(A : C|B) = H(AB) + H(BC) - H(B) - H(ABC)$ , where  $H(X)$  denotes the Shannon entropy of the bits within region  $X$ . It decays with a length scale called the spacetime Markov length  $\xi_p$ . (b) The mapping of the error threshold to a mixed-state phase transition. The circuit can be mapped to a resource state for MBQC. Measurements of the resource state decohere the state to create a mixed state. Noise in the circuit maps to noise acting on the mixed state, which can drive a mixed-state phase transition occurring at the same point as the circuit threshold. The Markov length diverges at the mixed-state phase transition, signaling a similar divergence of the spacetime Markov length at the fault-tolerance threshold.

manifest in measurement-based quantum computation (MBQC), where the time dimension of a quantum error-correcting process is replaced with an extra spatial dimension [44–46]. More specifically, the spacetime quantum circuit on a system with  $D$  spatial dimensions is realized by performing measurements on a resource state in  $D + 1$  spatial dimensions.

In this work, we leverage ideas from MBQC to map stabilizer codes with both physical and measurement errors to the mixed-state phases of decohered resource states. One key insight gained from this mapping is that methods used to probe the mixed-state phase transition can be employed as diagnostics for fault tolerance. In partic-

\* anegari@pitp.ca

ular, the conditional mutual information (CMI), defined as  $I(A : C|B) = S(AB) + S(BC) - S(B) - S(ABC)$  for the annular tripartition in Fig. 1, has proven useful for detecting mixed-state phase transitions [16]. In particular, when the CMI decays exponentially  $I(A : C|B) \sim e^{-\text{dist}(A,C)/\xi}$ , it defines a length scale  $\xi$ , dubbed the Markov length. The Markov length detects mixed-state phase transitions driven by local Lindbladians such as local dephasing; it is finite within each mixed-state phase but diverges at transitions [16]. The mapping motivates an analogous quantity for the stabilizer circuit, defined by the CMI of the (classical) syndrome distribution (Fig. 1). We show that through the mapping afforded by MBQC, the divergence of the associated length scale, which we call spacetime Markov length, signals the breakdown of fault tolerance. This correlation measure does not depend on any choice of decoder and probes the intrinsic fault-tolerance threshold.

The organization of the text is as follows. We first provide a definition of mixed-state phases in terms of local Lindbladian evolutions and in particular, emphasize that CMI is an important measure for detecting transitions [16]. We then review the foliation of syndrome-extraction circuits into resource states, demonstrating that faults in the original circuit correspond to applying noise to the resource state. Implementing the circuit corresponds to measuring all the bulk qubits of the resource state, thus leading to a decohered resource state due to both noise and measurements.

We then link the fault tolerance of the circuit to the ability to reverse the effects of noise on the decohered resource state. This allows us to identify the fault tolerance of the circuit with the condition that the decohered resource state is in the same mixed state phase as the noiseless, albeit measurement-decohered, resource state. Subsequently, we map the CMI of the decohered mixed state back to the circuit model, in which it becomes the CMI of the classical data extracted from the spacetime history of syndrome measurements. This sets a length scale—the spacetime Markov length—which diverges at the error threshold. Finally, we discuss the experimental relevance of this diagnostic as well as applications of decoherence in probing higher-form symmetry-protected topological (SPT) phase transitions.

**Mixed state phases and Markov length:** We begin by reviewing a definition of mixed-state phases and the role played by the CMI. For pure ground states of local Hamiltonians, two states are in the same phase of matter if they can be connected by finite-time evolution with a local (time-dependent) Hamiltonian. For mixed states, it is natural to generalize from a local Hamiltonian to a local Lindbladian evolution. However, since such dynamics is generally irreversible, one requires the existence of both a forward and reverse evolution with local Lindbladians. That is, there needs to exist local Lindbladians  $\mathcal{L}_1$  and  $\mathcal{L}_2$  such that  $\mathcal{T}e^{\int_0^1 \mathcal{L}_{1,2}(t)dt}[\rho_{1,2}] = \rho_{2,1}$  to conclude that  $\rho_1$  and  $\rho_2$  are in the same phase [11].

Given two mixed states in the same phase, finding the two-way evolutions connecting them can be challenging, and may require real-space renormalization or quantum error correction [15]. However, in many contexts, one is already given a one-way evolution  $\rho_p \equiv \mathcal{T}e^{\int_0^t \mathcal{L}_1(t)dt}[\rho_1]$  (e.g. a noisy  $\rho_1$ ) and the question of whether  $\rho_1, \rho_p$  are in the same phase reduces to whether the noise can be undone (is there a local Lindbladian evolution from  $\rho_p \rightarrow \rho_1$ ). To avoid having to find a reverse connection on a case by case basis, ideally one would like a criteria for the evolving state  $\rho_p$  that guarantees the existence of a reverse evolution. In other words, it is desirable to find a mixed-state analogue of a gap for ground states of local Hamiltonians; as long as the gap remains nonzero upon perturbing the Hamiltonian, the corresponding family of ground states are guaranteed to be in the same phase [47, 48].

In Ref. [16], it was found that the Markov length  $\xi$ , i.e., the length scale at which CMI decays—plays the role of the (inverse) gap for mixed states. Given a tripartition  $ABC$ , CMI is  $I(A : C|B) = I(A : BC) - I(A : B)$ , a difference of two mutual informations  $I(A : B) = S(A) + S(B) - S(AB)$ . This representation shows that CMI quantifies how much correlation between  $A$  and its complement is not captured by its correlations with  $B$ . CMI is intimately tied to the recoverability of a state from a subsystem: when CMI is small, there exists an approximate recovery channel  $\mathcal{R}_{B \rightarrow AB}$  such that  $\rho_{ABC} \approx \mathcal{R}_{B \rightarrow AB}[\rho_{BC}]$ . Hence, if CMI decays rapidly, then a local channel acting on  $A$  can be reversed by a channel acting on a relatively small buffer region  $B$ . Concretely, Ref. [16] used the approximate Petz theorem to argue that any local Lindbladian evolution in which the Markov length remains finite can be reversed by another local Lindbladian, where the locality of the reversal is determined by the Markov length along the evolution path. Thus, if a state evolving under a local Lindbladian has a finite Markov length, then all states along the path remain within the same mixed-state phase.

As an example of a mixed state phase transition, consider the two-dimensional toric code subject to bit-flip noise. The toric code Hamiltonian is  $H_{\text{t.c.}} = -\sum_{\square} A_{\square} - \sum_{+} B_{+}$ , where  $A_{\square} = \prod_{i \in \square} X_i$  and  $B_{+} \equiv \prod_{i \in +} Z_i$ . With periodic boundary conditions, its ground state subspace is four-dimensional, encoding two logical qubits with logical operators  $\tilde{X}_{v,h}, \tilde{Z}_{v,h}$  consisting of products of Pauli  $X$  and  $Z$  operators, respectively. Given perfect measurements of the syndromes  $A_{\square}, B_{+}$  and uniform bit-flip noise with probability  $p$ , for  $p > p_c \approx 0.11$ , the logical  $\tilde{Z}$  information is no longer decodable from the measurement outcomes. However, logical  $\tilde{X}$  commute with the noise channel and are thus decodable for all  $p$ .

This decodability transition manifests as a mixed state transition in the following sense. Given a ground state of the toric code  $|\text{t.c.}\rangle$ , the bit-flip noise converts it into a mixed state  $\rho_p \equiv \mathcal{E}_p^x[|\text{t.c.}\rangle\langle\text{t.c.}|]$ . Here,  $\mathcal{E}_p^x[\cdot] \equiv (1-p)(\cdot) + pX(\cdot)X$  is a bit-flip channel on every site that can be represented by a continuous Lindbladian evolution

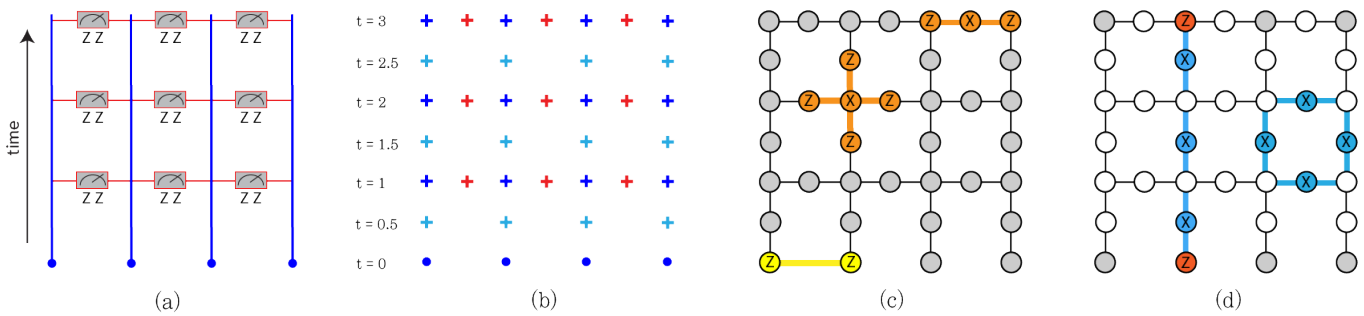


FIG. 2. Mapping the syndrome-extraction circuit of the 1D repetition code to a 2D mixed state. (a) The syndrome-extraction circuit is composed of  $Z_i Z_{i+1}$  measurements. (b) The resource state for MBQC is defined on copies of code qubits (blue) and syndrome qubits (red). The layers are labeled by integers and half-integers. There are no syndrome qubits in the  $t = 0$  layer, as the input code state is assumed to be perfect. (c) The qubits are entangled into a cluster state by applying CZ gates to neighboring qubits, with stabilizers indicated. (d) Measuring the bulk in the  $X$  basis produces a mixed state coupled to the original code on the boundaries: the resulting ensemble is stabilized by local plaquette operators and composites of the logical operators of the bulk and boundary codes.

$\mathcal{L}[\rho] = \sum_i \frac{1}{2} (X_i \rho X_i - \rho)$  for time  $t_p = -\ln(1 - 2p)$ . The Markov length of the mixed state  $\rho_p$  is finite everywhere except  $p_c \approx 0.11$ , at which it diverges [16]. Hence, the mixed state phase transition as defined by two-way local Lindbladian connectivity to the initial state  $\rho_0$  coincides with the decodability transition.

For  $p > p_c$ , the fact that Markov length is finite implies that  $\rho_p$  are in the same phase as  $\rho_{cl} \equiv \rho_{p=0.5} = \left(\prod \frac{1+A\Box}{2}\right) \rho_{\tilde{X}}$ , which is an ensemble of loop configurations in the  $X$  basis and  $\rho_{\tilde{X}}$  depends on the initial logical state. The classical ensemble with definite logical  $\tilde{X}$  operators (e.g.  $\tilde{X}_{v,h} = +1$ ) is preparable from a product state by a local Lindbladian [16] and thus in the trivial phase under the definition in [11].

However, the classical ensemble  $\rho_{cl}$  is non-trivial in several senses, which will be important for the purposes of our work. Most importantly, it is a topological classical memory with logical information given by  $\tilde{X}_{v,h} = \pm 1$ , and the logical states  $\left(\prod \frac{1+A\Box}{2} \prod_{l=v,h} \frac{1\pm\tilde{X}_l}{2}\right)$  are locally indistinguishable. This topological degeneracy is preserved under any local Lindbladian evolution in which Markov length remains finite [49]; the approximate Petz recovery for such an evolution only depends on local reduced density matrices which are the same for all topologically degenerate states. This reverse evolution thus serves as a decoder that recovers the initial state (and any logical information encoded therein) [16]. Hence, any finite-time Lindbladian evolution connecting non-trivial to trivial topological degeneracy must produce a diverging Markov length at some point [49].

This motivates the following refined definition for mixed state phases:

**Definition** ([49]).  $\rho_{1,2}$  are in the same mixed state phase if  $\rho_2 = \mathcal{T}e^{\int_0^1 \mathcal{L}(t)dt}[\rho_1]$  for a local Lindbladian  $\mathcal{L}$  and  $\mathcal{T}e^{\int_0^{t'} \mathcal{L}(t)dt}[\rho_1]$  has finite Markov length for all  $t' \leq 1$ .

Under this refined definition, the classical state  $\rho_{cl}$  is non-trivial. Indeed, upon applying a dephasing channel

$\mathcal{E}_p^z[\cdot] \equiv (1-p)(\cdot) + pZ(\cdot)Z$ , the state  $\rho_{cl,p} \equiv \mathcal{E}_p^z[\rho_{cl}]$  undergoes a phase transition to a trivial phase at  $p_c \approx 0.11$ , at which the Markov length diverges.

**Mapping circuits to mixed states:** Here, we describe how a circuit for syndrome extraction can be mapped to a mixed state. The first step is to map the circuit to a resource state for MBQC. This can be accomplished using the notion of foliation, introduced in Refs. [45, 46]. For simplicity, we restrict our attention to syndrome-extraction circuits for stabilizer codes and subsystem codes in  $D$  dimensions with geometrically local checks. In this case, foliation produces a resource state in  $D + 1$  dimensions, which is short-range entangled in the bulk. Performing measurements on the resource state then reproduces the effects of the circuit and produces a mixed state according to the distribution of measurement outcomes. Note that, for simplicity, we consider Calderbank-Steane-Shor (CSS) codes throughout the text. We fully expect that the discussion can be extended to non-CSS codes using the generalizations in Ref. [46].

*Circuit to resource state* – Following Ref. [46], the resource state for MBQC is defined in a Hilbert space composed of two layers of qubits for every implementation of the circuit. This is depicted in Fig. 2 for the 1D repetition code. The two layers correspond to the  $Z$ -checks and  $X$ -checks of the syndrome-extraction circuit, respectively. We refer to the layers by integers and half-integers, so that the  $m$  and  $m + \frac{1}{2}$  layers define the  $m^{\text{th}}$  application of the circuit, for  $m \in \mathbb{Z}$ . We take the initial implementation of the circuit to be the  $t = 0$  and  $t = \frac{1}{2}$  layers, while the final implementation is  $t = m_f$ , for some  $m_f \in \mathbb{Z}^+$ . Note that we do not include a layer for  $m_f + \frac{1}{2}$ .<sup>1</sup>

Each layer is comprised of two types of qubits. First, each layer hosts a copy of the code qubits, so that the

<sup>1</sup> This is primarily so that, if the resource state is extended to larger  $t$ , we can take  $m_f$  to be the initial integer layer.

Hilbert space of the input code is reproduced in each layer. Second, there is a syndrome qubit for every check, with the placement of the syndrome qubit depending on the type of check. For the  $Z$ -type checks, we place the syndrome qubit in the integer layers, while for the  $X$ -type checks, the qubit is placed in the half-integer layers. Note that, for classical codes (with only  $Z$ -type checks), such as the repetition code, there are no syndrome qubits in the half-integer layers.

To build the resource state, we next need to specify an initial state for the code qubits in the  $t = 0$  layer. The choice of initial state is dependent on the context. If, for example, the circuit is being used for state preparation, then the initial state may be a product state. Here, we take the initial state to be a code state, and interpret the circuit as implementing a quantum memory. We assume that the initial code state has been prepared fault tolerantly, prior to applying the syndrome-extraction circuit.

The final step is to prepare all of the qubits (except for the code qubits in the  $t = 0$  layer) in the  $|+\rangle$  state and couple them together with  $CZ$  gates. Specifically, we apply a  $CZ$  gate between each code qubit in the layer  $t$  and its copies in the neighboring  $t - \frac{1}{2}$  and  $t + \frac{1}{2}$  layers.<sup>2</sup> We also apply a  $CZ$  gate between each syndrome qubit and the code qubits of the corresponding check. Thus, in the bulk, the state is a graph state. This completes the construction of the resource state. The resource state for the 1D repetition code is shown in Fig. 2.

*Resource state to mixed state* – Now that we have defined the resource state for MBQC, we are able to finish the mapping of the syndrome-extraction circuit to a mixed state. In practice, the syndrome-extraction circuit is implemented within the MBQC formalism by measuring all of the qubits in the  $X$  basis, except for the code qubits in the final layer, that is,  $t = m_f$ . Given that the measurement outcomes are probabilistic, this produces a mixed state that is a classical distribution of the  $X$  basis states (except on the code qubits at  $t = m_f$ ).

The effect of measuring the single-site  $X$  operators is equivalent to adding full-strength bit-flip noise to the resource state.<sup>3</sup> Therefore, letting  $\rho_{RS}$  denote the resource state, the mixed state obtained after the measurements is:

$$\rho_0 \equiv \mathcal{E}_{p=\frac{1}{2}}^x(\rho_{RS}). \quad (1)$$

Here, the channel  $\mathcal{E}_{p=\frac{1}{2}}^x$  is the full-strength bit-flip channel, which, for each site, applies a Pauli  $X$  operator with probability  $p = \frac{1}{2}$ . Implicitly,  $\mathcal{E}_{p=\frac{1}{2}}^x$  acts on every qubit except for the code qubits in the final layer  $t = m_f$ .

To gain intuition for the mixed state  $\rho_0$ , we consider the bulk state  $\rho_{cl} = \text{Tr}_{m_f}(\rho_0)$ , where we have traced out

the top layer  $t = m_f$ . The state  $\rho_{cl}$  is a purely classical state. This is because, due to the full-strength bit-flip noise, the state  $\rho_{cl}$  commutes with every single-site  $X$  operator. Therefore,  $\rho_{cl}$  is diagonal in the  $X$  basis, i.e., it is a mixture of  $X$  basis states. For example, starting with the 1D repetition code, the state  $\rho_{cl}$  is a mixture of loop configurations, where the loops are formed by  $|-\rangle$  states on the dual lattice. We argue below that the threshold of the underlying quantum code coincides with a phase transition in the bulk of the mixed state  $\rho_0$ .

**Mapping noisy circuits to noisy states:** We demonstrate that noise in the circuit model corresponds to the evolution of the mixed state  $\rho_0$  under a particular local Lindbladian. This naturally motivates the question of whether the mixed state undergoes a phase transition induced by the Lindbladian evolution. In the sections that follow, we argue that the question is equivalent to identifying whether a threshold exists for the syndrome-extraction circuit and furthermore that the mixed-state phase transition coincides with the threshold.

Consider an  $X$  or  $Z$  error occurring on a code qubit  $i$  between two consecutive implementations of the circuit, denoted by  $t$  and  $t+1$ . As discussed previously, each time step  $t$  in the circuit corresponds to two time steps in the resource state, specifically  $t$  and  $t + \frac{1}{2}$ . This mapping yields the following translation of errors:

1. **Circuit  $X$  error:** This becomes a  $Z$  error in the resource state at time step  $t + \frac{1}{2}$  on the corresponding code qubit  $i$ .
2. **Circuit  $Z$  error:** This becomes a  $Z$  error in the resource state at time step  $t + 1$  on the corresponding code qubit  $i$ .
3. **Readout error:** This becomes a  $Z$  error on the corresponding syndrome qubit of the resource state.

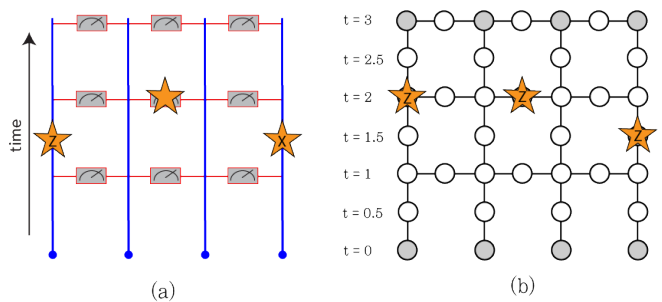


FIG. 3. Error mapping from the syndrome-extraction circuit to the resource state for the 1D repetition code. Error locations are denoted by stars and are translated to the MBQC setting according to rules 1-3. in the main text.

To understand this noise mapping, it is instructive to examine how qubit  $i$  is teleported from time  $t$  to  $t + 1$ . As described in Ref. [7, 46], this is achieved by measuring this code qubit at times  $t$  and  $t + \frac{1}{2}$ . After these two

<sup>2</sup> Here,  $t$  ranges from  $0 < t < m_f$ .

<sup>3</sup> This can be seen directly for a single qubit in the state  $\rho$ , since the post-measurement state is  $\frac{1+X}{2}\rho\frac{1+X}{2} + \frac{1-X}{2}\rho\frac{1-X}{2}$ , which is equal to  $\frac{1}{2}\rho + \frac{1}{2}X\rho X$ .

measurements, the state of code qubit  $i$  at time  $t$  is teleported to time step  $t + 1$ , though with a Pauli correction depending on the measurement results. Let us denote the two measurement results by  $s_{i,t}$  and  $s_{i,t+\frac{1}{2}}$ , where they take the value 0 when the outcome is the  $|+\rangle$  state and 1 when the outcome is the  $|-\rangle$  state. These measurement results alter the teleported state at time  $t + 1$  by the action of the extra Pauli operators  $Z^{s_{i,t}} X^{s_{i,t+\frac{1}{2}}}$ .

This demonstrates that changing the value of the measurement result at integer time will manifest as an additional  $Z$  operator acting on the teleported state, while changing the result at half-integer time will result in an additional  $X$  operator acting on the state. The change in the measurement results can be viewed as a  $Z$  error on a code qubit, as this flips the value of  $s$ . Furthermore, a  $Z$  error on the syndrome ancilla flips the outcome of the  $X$  measurement, manifesting as a readout error. This unifies all stochastic circuit errors as  $Z$ -dephasing errors in the resource state, with other types of errors appearing as correlated errors.

If these errors occur randomly in the circuit model with probability  $p$ , they will similarly manifest in the resource state with probability  $p$ . (For simplicity, we assume Pauli noise and readout error occur with the same probability, but the mapping readily generalizes.) Therefore, the resource state undergoes a dephasing channel  $\mathcal{E}_p^z(\cdot) = (1-p)(\cdot) + pZ(\cdot)Z$ , on the syndrome qubits and code qubits depending via the above map on the type of Pauli error. The resulting mixed state after both noise and measurement is

$$\rho_p \equiv \mathcal{E}_{p=\frac{1}{2}}^x(\mathcal{E}_p^z(\rho_{RS})) = \mathcal{E}_p^z(\rho_0), \quad (2)$$

as  $\mathcal{E}_p^z, \mathcal{E}_{p=1/2}^x$  commute.

### Fault tolerance and mixed-state phase transition:

We now establish a connection between the fault tolerance of the syndrome-extraction circuit and the mixed-state phases of the measured resource state. We begin by showing that the fault tolerance of the circuit is equivalent to the fault tolerance of the corresponding MBQC protocol.

We consider a circuit or an MBQC protocol fault tolerant if they admit an error threshold for successful recovery (with a realistic error model) and they are implemented below threshold for a sufficiently large system size. Given a noisy circuit with error rate  $p$ , we let  $\tilde{\rho}_p = \sum_{\vec{s}} p_{\vec{s}} |\vec{s}\rangle\langle\vec{s}| \otimes \rho_{t,\vec{s}}$  denote the mixture of all possible syndromes  $\vec{s}$ , weighted by their probabilities  $p_{\vec{s}}$ , with the corresponding final states  $\rho_{t,\vec{s}}$  of the circuit. Fault tolerance then requires the existence of a recovery map  $\tilde{R}$  such that  $\tilde{R}(\tilde{\rho}_p) \approx \tilde{\rho}_0$  for  $p < p_c$ , where  $p_c$  denotes the noise threshold and  $\tilde{R}$  is independent of the encoded information.<sup>4</sup> Similarly, fault tolerance in the MBQC

setting requires the existence of a recovery map  $R$  such that  $R(\rho_p) \approx \rho_0$  for  $p < p_c$ .

Fault tolerance in the circuit and MBQC setting are equivalent because the existence of a recovery channel  $R$  yields a recovery channel  $\tilde{R}$  for the corresponding circuit, and vice-versa. To see this, we first note that the state  $\tilde{\rho}_p$  corresponds to the state  $\rho_p$  when the code qubits are post-selected in the  $|+\rangle$  state within the bulk. This post-selection can be implemented through a feedback channel  $F$ , such that  $F(\rho) = \tilde{\rho}$ . The feedback channel measures all bulk code qubits, obtaining outcomes  $\vec{C}$ , and applies unitary corrections  $U_{\vec{C}}$  to all syndrome and code qubits, conditioned on the outcomes. The feedback channel can be inverted ( $\rho = F^{-1}(\tilde{\rho})$ ), where  $F^{-1}$  applies  $U_{\vec{C}}^{-1}$  with probability 1/2. Therefore, the circuit and MBQC recovery maps are related by:

$$\tilde{R} = F \circ R \circ F^{-1}. \quad (3)$$

This allows us to relate the threshold of the circuit to the mixed-state phase transition of  $\rho_p = \mathcal{E}_p^z(\rho_0)$ . These states are always one-way connected from  $\rho_0$  by the noise channel  $\mathcal{E}_p^z$ , and the question of whether they are in the same phase thus hinges on the existence of a recovery  $R$ , which guarantees a circuit recovery  $\tilde{R}$  as we showed.

We first prove by contradiction that the Markov length diverges at the error threshold for the circuit. Assume instead that the Markov length remains finite at  $p_c$  and within an  $\epsilon$ -neighborhood around  $p_c$ . Given the noise channel evolving the density matrix  $\rho_p$  from  $p = p_c - \epsilon$  to  $p = p_c + \epsilon$ , a finite Markov length in this region implies that a reverse Lindbladian can be constructed, evolving the density matrix from  $p_c + \epsilon$  back to  $p_c - \epsilon$ . This reverse Lindbladian evolution, when combined with the recovery map  $R$  below the threshold, would enable recovery<sup>5</sup> above  $p_c$ , contradicting the assumption that  $p_c$  represents the true threshold.

While this argument is sufficient to show that the Markov length diverges at  $p_c$ , it does not exclude the possibility of divergence at multiple points. However, we expect that this generically does not happen, based on mapping the problem of recovery to statistical-mechanics models [50]. In this mapping, the (dis)ordered phase of the stat mech model corresponds to the (un)recoverable regime. CMI corresponds to the free energy cost of a point defect in the stat mech model [16], and thus, the

---

correct all errors. In practice, there can be residual uncorrected errors that can be handled in future iterations of the circuit. Hence we disregard these residual errors by assuming that no errors occur in the final round of the circuit. Equivalently, for MBQC, this corresponds to the noise channel  $\mathcal{E}_p^z$  acting on all qubits except those at the top boundary.

<sup>5</sup> Note that the combination of the reverse Lindbladian and a sub-threshold recovery is a valid recovery because the approximate Petz recovery of the reverse Lindbladian depends solely on local reduced density matrices, which are independent of the encoded logical information of the underlying topological code.

---

<sup>4</sup> This recovery condition assumes that the fault-tolerant circuit

Markov length can be identified with the correlation length—assuming that there is only one diverging length scale in the vicinity of the critical point of the stat mech model. As a consequence, the divergence of the Markov length coincides with the recoverability transition.

**Classical memory in the bulk:** Here we analyze the above mixed-state phase transition in more detail and connect the fault tolerance of the circuit to the recoverability of a classical memory in the bulk of the decohered resource state. We identify two important classes of stabilizers of the resource state, which we refer to as *detector cells* and  $L'BL$ , which define the bulk classical memory.

*Detector cells* – The first type of stabilizers, referred to as detector cells following Refs. [51, 52], capture the redundancy inherent to the circuit. Without errors, consecutive measurements of a stabilizer yield consistent syndromes. For instance, in the repetition code, the measurements of the stabilizer  $Z_i Z_{i+1}$  at times  $t$  and  $t+1$  should agree in the absence of errors. In MBQC, this process is equivalent to measuring the  $X$  operator on the syndrome qubit associated with the stabilizer. Measuring  $X_i$  and  $X_{i+1}$  on the code qubits in the intermediate layer ( $t + \frac{1}{2}$ ) teleports the stabilizer from  $t$  to  $t+1$ , possibly with a sign change  $X_i X_{i+1}$ . Finally, measuring  $X$  on the syndrome qubit at  $t+1$  yields a second syndrome measurement, influenced solely by the teleportation-induced sign change. Thus, assuming no errors, the product of these  $X$  measurements should yield  $+1$ . This detector cell is depicted in Fig. 2(d) as a plaquette of  $X$  operators.

In general, for a stabilizer  $S$  measured in the circuit, the corresponding detector cell is:

$$D_S = \left( \prod_{i \in \text{Ch}(S)} X_i^{(t+1)} \right) \left( \prod_{i \in \text{Sup}(S)} X_i^{(t+\frac{1}{2})} \right) \left( \prod_{i \in \text{Ch}(S)} X_i^{(t)} \right). \quad (4)$$

Here,  $\text{Ch}(S)$  is a choice of syndrome qubits such that the product of the corresponding checks is  $S$ ,<sup>6</sup> and  $\text{Sup}(S)$  is the set of code qubits in the support of  $S$ . Measuring  $X$ -operators on  $\text{Sup}(S)$  in the intermediate layer  $t + \frac{1}{2}$  teleports the stabilizer  $S$  from layer  $t$  to  $t+1$ , with the  $X$ -measurements at  $t+1$  providing a second syndrome consistent with that at  $t$ .<sup>7</sup>

*L'BL stabilizers* – The second type of stabilizer arises from the temporal consistency of logical operators. Without noise, the logical information encoded in the code at

different time instances should agree. Consider two instances of a repetition code logical operator,  $Z_i^{(m_f)}$  and  $Z_i^{(0)}$ , acting on the code qubits in the final and initial layers of the circuit. The temporal consistency of this logical is reflected in the resource state through a stabilizer of the following form:

$$L_{m_f}^Z B_{L^Z} L_0^Z = Z_i^{(m_f)} \left( \prod_{k=0}^{m_f-1} X_i^{(k+\frac{1}{2})} \right) Z_i^{(0)},$$

Here, the logical operators  $L_{m_f}^Z$  and  $L_0^Z$  are linked via the operator  $B_{L^Z}$ , which acts within the bulk of the state. This stabilizer is illustrated in Fig. 2(d), where the supports of  $L_{m_f}^Z$  and  $L_0^Z$  are highlighted in red, and the support of  $B_{L^Z}$  is depicted in blue. We refer to these as  $L'BL$  stabilizers, for simplicity.

In general, the resource state has stabilizers of the form  $L_{m_f} B_L L_0$ , with  $B_L$  given by

$$B_{L^Z} = \prod_{k=0}^{m_f-1} \prod_{i \in \text{Sup}(L^Z)} X_i^{(k+\frac{1}{2})}, \quad (5)$$

$$B_{L^X} = \prod_{k=0}^{m_f-1} \prod_{i \in \text{Sup}(L^X)} X_i^{(k)},$$

depending on whether the logicals  $L_0, L_{m_f}$  are products of Pauli  $Z$  or  $X$  operators.

*Classical memory in the bulk* – We now explain how the  $B_L$  and  $D_S$  operators together define a classical memory. In this memory, the  $D_S$  operators act as the check operators, while the  $B_L$  operators represent the logical bits. Both  $D_S$  and  $B_L$  are products of  $X$ -type operators and thus commute. Moreover, the  $B_L$  operators are independent of the  $D_S$  operators because logical bits represented by  $B_L$  can be flipped by conjugating them with  $L_m$  or  $L_{m-\frac{1}{2}}$ ,<sup>8</sup> while the  $D_S$  operators remain invariant (a logical error does not alter the values of detector cells).

For example, the bulk code derived from the repetition code has plaquettes of  $X$ -type operators serving as checks and open strings of  $X$ -type operators connecting one boundary to another as logical operators, as depicted in Fig. 2. The code distance scales linearly with the system size, as non-contractible closed loops of  $Z$ -errors can alter the logical bit without being detected by the checks. Note that for the 1D repetition code, there is only one bit encoded, corresponding to the operator  $B_{L^Z}$ . In contrast, there is no bit corresponding to the operator  $B_{L^X}$ , as the repetition code is designed to protect against  $X$ -type noise only.

*Error correction and fault tolerance* – We now analyze how the error correction properties of this classical code

<sup>6</sup> Note that the choice of syndrome qubits is for subsystem codes in particular, where different choices of gauge operators may multiply to the same stabilizer.

<sup>7</sup> Detector cells can also correspond to local redundancy checks within a single layer. For example, in the 3D toric code, there are detector cells represented by the product of plaquette stabilizers around a cube. However, we do not explicitly discuss these types of detector cells here, for simplicity.

<sup>8</sup> Here,  $L_m$  and  $L_{m-\frac{1}{2}}$  are the logical operators of the underlying code defined within the  $m$  and  $m - \frac{1}{2}$  layers of the resource state, respectively.

relate to the fault tolerance of the circuit. Let us begin with the noiseless scenario. In this case, transmitting a logical state from one boundary to another in MBQC can be understood as a two-step process. First, measurements in the bulk establish entanglement between the top and bottom boundaries. Then, measuring the bottom boundary teleports the information to the top boundary, upon applying feedback depending on all measurement outcomes.

The  $L'BL$  stabilizer enables this teleportation process. The initial state satisfies  $L'BL = 1$ , and measuring the bulk corresponds to measuring the  $B$  operators. Consequently, the state on the boundaries is stabilized by  $L'L$ , taking value  $B$ . Successfully teleporting the logical state from one boundary to the other requires feedback depending on the measured value of  $B$ .

In the presence of noise, the errors need to be removed while preserving  $L'BL$ ; otherwise the feedback is wrong. The condition for removing errors without changing a logical operator  $B$  is precisely the condition for the classical memory to persist in the presence of noise. Thus, retention of classical memory implies the ability to teleport the logical state from the initial boundary to the final boundary, which in turn implies preservation of logical information in the original circuit.

As an example, the threshold for the 1D repetition code with probability  $p$  for both bit-flip and readout error maps to the threshold for the 2D classical memory defined by  $\rho_{cl} = \left(\prod \frac{1+A\Box}{2}\right)\rho_{\tilde{X}}$  subject to dephasing noise  $\mathcal{E}_p^z$ . We note that [40] offers a complementary approach to our mixed state phase perspective, using strange correlators of the noisy cluster state to diagnose its ability to transmit information from one boundary to the other.

*Higher-Form Symmetries* – In some cases, the detector cells generate higher-form symmetries, i.e., for which the symmetry operators are supported on closed submanifolds, as described in Ref. [53]. In particular, when the stabilizers generate a  $q$ -form symmetry, the detector cells then generate a  $q$ -form symmetry in one dimension higher. For example, the stabilizers of the toric code generate a  $\mathbb{Z}_2 \times \mathbb{Z}_2$  1-form symmetry. Correspondingly, the detector cells of the foliated state also generate a  $\mathbb{Z}_2 \times \mathbb{Z}_2$  1-form symmetry—this is the well-known  $\mathbb{Z}_2 \times \mathbb{Z}_2$  1-form symmetry of the 3D cluster state [54]. Thus, in this case, the redundancy of the stabilizer measurements produces a higher-form symmetry of the resource state.

This contrasts with cases such as the Bacon-Shor code, which is not fault tolerant. In that case, the detector cells of the resource state are rigid, in the sense that they are linear subsystem symmetries of the resource state. We postulate that, if the checks are local, then higher-form symmetries of the resource state are necessary for fault tolerance.

In the case that the stabilizers of the underlying code generate an anomalous  $q$ -form symmetry, then the stabilizers of the form  $L'BL$  are an indication that the resource state belongs to a nontrivial  $q$ -form SPT phase. The  $L'BL$  operators imply that the symmetry defects of

the  $q$ -form symmetry (created by  $B$ ) are dressed with  $q$ -form symmetry charges, given by  $L'$  and  $L$ . This is because the operator  $L_m$  ( $L_{m-\frac{1}{2}}$ ) defined by the logical operator  $L^Z$  ( $L^X$ ) fails to commute with  $B_{L^X}$  ( $B_{L^Z}$ ) when they have overlapping support and  $L^Z$  and  $L^X$  are conjugate logical operators.

For example, the stabilizers of the toric code generate an anomalous  $\mathbb{Z}_2 \times \mathbb{Z}_2$  1-form symmetry. The resource state is known to belong to a nontrivial 1-form SPT phase, as seen by the  $L'BL$  stabilizers. We refer to Refs. [54, 55] for further details.

**Spacetime Markov length:** We employ the Markov length as a diagnostic for a mixed-state phase transition to show that the CMI of the classical data extracted from a noisy circuit serves as an indicator of the error threshold. We begin by showing that the CMI of a decohered resource state depends exclusively on the entropy of specific detector cells. We then demonstrate a parallel result for the circuit itself, where the CMI of classical syndromes depends solely on the entropy of the corresponding classical bits associated with the detector cells. Finally, we prove that under the noise mapping, the entropy of the resource state's detector cells matches the entropy of their circuit counterparts. This correspondence establishes an equality between the CMI of the decohered resource state and that of the classical data, thereby confirming spacetime Markov length as a robust indicator of the error threshold.

We begin by examining a decohered resource state derived from the correspondence with a given quantum circuit. To quantify the CMI of this state, we compute the reduced density matrix for a given region  $A$  of the decohered resource state and analyze its entropy. Decohering the system in the  $X$ -measurement basis effectively removes all initial stabilizers of the state except the ones that commute with  $X$ -measurements. These stabilizers are composed of Pauli- $X$  operators and are the detector cells. Consequently, the reduced density matrix post-measurement (with discarded outcomes) assumes the form:

$$\rho_A = \frac{1}{N} \prod_k \frac{1 + D_k}{2}, \quad (6)$$

where  $N$  is a normalization factor, and  $D_k$  are stabilizers corresponding to detector cells inside the region.<sup>9</sup>

Introducing a noise channel with strength  $p$  to this reduced density matrix modifies it to:

$$\rho_{A,p} = \frac{1}{N} \sum_{m_k} P_{m_k} \prod_k \frac{1 + m_k D_k}{2}, \quad (7)$$

<sup>9</sup> In general, non-local symmetries may exist within a given region, particularly for regions that are not simply connected; however, we still refer to these as detector cells.

where  $P_{m_k}$  represents the probability distribution over the sign of detector cells ( $m_k$ ) in the resource state. Computing the von Neumann entropy of this density matrix gives:

$$S(\rho_{A,p}) = H(m) + |A| - |D| \quad (8)$$

This has two contributions: the first is the Shannon entropy of the probability distribution of the sign distribution,  $H(m) = -\sum P_{m_k} \log P_{m_k}$ , and the second is a term from the normalization factor  $N$ , which depends on the number of qubits inside the region ( $|A|$ ) and the number of detector cells within it ( $|D|$ ).

Next, we examine the corresponding region  $A$  in the circuit. In a noise-free scenario, the extracted syndromes have deterministic components that correspond to detector cells in the resource state. For instance, consider two syndromes  $s_1$  and  $s_2$  that are outcomes of repeated measurements of a given stabilizer. From the consistency of the result in the noise-free scenario, we know  $s_1 = s_2$  which means  $d_1 = s_1 s_2$  is a deterministic variable. Given a bit string  $s_i$  from region  $A$ , the syndromes can be expressed in terms of deterministic components  $d_i$  and a basis for non-deterministic components  $n_i$ . The non-deterministic syndromes remain completely random, even under stochastic errors, as seen from the stabilizer formalism. Thus, the entropy of  $s_i$  includes two contributions: one from the deterministic components  $d_i$  and another from the fully random components  $n_i$ . Stochastic errors turn the deterministic components  $d_i$  into random variables, with probability distribution  $P(d_1, d_2, \dots, d_k)$ . This yields the total entropy:

$$H(s) = H(d) + |s_i| - |d_i|, \quad (9)$$

where  $H(d)$  represents the entropy of the  $d_i$  values, and the second two terms account for the  $|n_i|$  fully random variables within the region.

The correspondence between detector cells in the resource state and deterministic components in the circuit implies  $|d_i| = |D|$ , and the noise mapping ensures that any error changing the sign of a detector cell also changes the sign of the corresponding deterministic component. This shows that the probability distribution of the sign of detector cells  $P_m$  matches that of the deterministic components  $P_d$ , so  $H(m) = H(d)$ . Because the volume law terms  $|s_i|$  and  $|A|$  do not contribute to CMI, this establishes the equality of CMI between the circuit and MBQC.

**Discussion:** We have shown that the breakdown of fault tolerance in local stabilizer quantum memories can be mapped to mixed state transitions of classical memories in one higher dimension. This mixed-state perspective offers the novel diagnostic of the spacetime Markov length, which can be computed directly from the syndrome distribution of the circuit. This diagnostic does not depend on any decoder and thus probes the intrinsic threshold transition.

As repetition and surface codes below the noise threshold have been realized recently on quantum hardware [56], it would be very interesting to extract the spacetime Markov length from experimental syndrome data as a complementary probe of the proximity to the threshold. Real-time decoders acting in parallel on spacetime blocks (and then finding a globally consistent solution) have been demonstrated [56]. The spacetime Markov length scale, in particular, may be useful to estimate the minimum block sizes for such decoders.

This approach can also be applied to more general circuits that implement logical gates through code deformations, such as lattice surgery. These circuits define resource states where the logical gates are encoded into the geometry of the cluster state [46]. Further research could also investigate mixed-state phase transitions within the formalism of  $ZX$  calculus [57], which would generalize our analysis to inherently dynamical quantum-error correcting codes, such as Floquet codes [58]. Another promising direction is the exploration of spacetime circuit codes, where we anticipate that the outcome code [59] could serve a similar role as the classical memory in our analysis. In this context, error correction for the classical memory would be linked to fault tolerance, and the spacetime Markov length could once again be used to detect the threshold.

While this work focused on fault-tolerant stabilizer codes (and corresponding Clifford operations), it would be interesting to extend this approach to non-Abelian topological memories or operations beyond the stabilizer paradigm. The general case requires adaptive feedback from syndrome measurement, meaning that the mapping of a fault-tolerant circuit to a noisy resource state would be more complex. However, in this context, the spacetime Markov length may still be relevant. Fault tolerance with measurement errors relies on the redundancy of the syndromes, and thus it is plausible that the classical syndrome state must generally be non-trivial and spacetime Markov length may detect its transition to a trivial state.

*Application to higher-form SPT transitions:* We note that the measurements which decohere the resource state into a classical ensemble are essential for defining a mixed state phase transition. Without measurements, the resource state with periodic boundary conditions does *not*, in fact, undergo a phase transition when noise is applied. This is because a cluster state subject to local dephasing noise is equivalent to a thermal Gibbs state of the cluster-state Hamiltonian [27, 60], which has zero CMI [61].

The measurement decoherence which exposes the mixed state phase transition may be more generally useful in exposing “hidden” transitions of SPT phases protected by higher-form symmetries under both incoherent and coherent perturbations. For example, in Ref. [62], there are instances in which the higher-form symmetry protecting an SPT is explicitly broken, leading to no bulk phase transition but which still exhibits a boundary transition. The effect of the measurement decoherence in the symmetry-charge basis is to effectively



introduce a boundary after spacetime rotation [14], thus exposing the hidden transition.

**Acknowledgments:** AN thanks Ali Lavasani for valuable discussions. TDE acknowledges Lawrence Cohen, Dongjin Lee, Yaodong Li, Sam Roberts, Charles Stahl, and Dominic Williamson for work on related projects. TH thanks Tarun Grover, Leonardo Lessa, Roger Mong, Shengqi Sang, and Chong Wang for collaboration on re-

lated projects. This work was supported by the Perimeter Institute for Theoretical Physics (PI), the Natural Sciences and Engineering Research Council of Canada (NSERC), and an Ontario Early Researcher Award. Research at PI is supported in part by the Government of Canada through the Department of Innovation, Science, and Economic Development, and by the Province of Ontario through the Ministry of Colleges and Universities.

- 
- [1] D. Aharonov and M. Ben-Or, [Fault-tolerant quantum computation with constant error rate](#) (1999), [arXiv:quant-ph/9906129 \[quant-ph\]](#).
- [2] A. Kitaev, [Fault-tolerant quantum computation by anyons](#), *Annals of Physics* **303**, 2–30 (2003).
- [3] E. Knill, R. Laflamme, and W. H. Zurek, [Resilient quantum computation: error models and thresholds](#), *Proceedings of the Royal Society of London. Series A: Mathematical, Physical and Engineering Sciences* **454**, 365–384 (1998).
- [4] P. W. Shor, [Fault-tolerant quantum computation](#) (1997), [arXiv:quant-ph/9605011 \[quant-ph\]](#).
- [5] E. Dennis, A. Kitaev, A. Landahl, and J. Preskill, [Topological quantum memory](#), *Journal of Mathematical Physics* **43**, 4452–4505 (2002).
- [6] C. T. Chubb and S. T. Flammia, [Statistical mechanical models for quantum codes with correlated noise](#), *Annales de L'Institut Henri Poincaré D* **8**, 269 (2021).
- [7] J. Hauser, Y. Bao, S. Sang, A. Lavasani, U. Agrawal, and M. P. A. Fisher, [Information dynamics in decohered quantum memory with repeated syndrome measurements: a dual approach](#) (2024), [arXiv:2407.07882 \[quant-ph\]](#).
- [8] F. Verstraete, M. M. Wolf, and J. Ignacio Cirac, [Quantum computation and quantum-state engineering driven by dissipation](#), *Nature Physics* **5**, 633 (2009).
- [9] S. Diehl, A. Micheli, A. Kantian, B. Kraus, H. P. Büchler, and P. Zoller, [Quantum states and phases in driven open quantum systems with cold atoms](#), *Nature Physics* **4**, 878 (2008).
- [10] M. B. Hastings, [Topological order at nonzero temperature](#), *Physical review letters* **107**, 210501 (2011).
- [11] A. Coser and D. Pérez-García, [Classification of phases for mixed states via fast dissipative evolution](#), *Quantum* **3**, 174 (2019).
- [12] R. Fan, Y. Bao, E. Altman, and A. Vishwanath, [Diagnostics of mixed-state topological order and breakdown of quantum memory](#), *arXiv preprint arXiv:2301.05689* (2023).
- [13] Y.-H. Chen and T. Grover, [Separability transitions in topological states induced by local decoherence](#), *arXiv preprint arXiv:2309.11879* (2023).
- [14] Y. Bao, R. Fan, A. Vishwanath, and E. Altman, [Mixed-state topological order and the errorfield double formulation of decoherence-induced transitions](#) (2023), [arXiv:2301.05687 \[quant-ph\]](#).
- [15] S. Sang, Y. Zou, and T. H. Hsieh, [Mixed-state quantum phases: Renormalization and quantum error correction](#), *Phys. Rev. X* **14**, 031044 (2024).
- [16] S. Sang and T. H. Hsieh, [Stability of mixed-state quantum phases via finite markov length](#) (2024), [arXiv:2404.07251 \[quant-ph\]](#).
- [17] J. Y. Lee, C.-M. Jian, and C. Xu, [Quantum criticality under decoherence or weak measurement](#), *arXiv preprint arXiv:2301.05238* (2023).
- [18] Y. Zou, S. Sang, and T. H. Hsieh, [Channeling quantum criticality](#), *Physical Review Letters* **130**, 250403 (2023).
- [19] C. de Groot, A. Turzillo, and N. Schuch, [Symmetry protected topological order in open quantum systems](#), *Quantum* **6**, 856 (2022).
- [20] R. Ma and C. Wang, [Average symmetry-protected topological phases](#), *Physical Review X* **13**, 031016 (2023).
- [21] J.-H. Zhang, Y. Qi, and Z. Bi, [Strange correlation function for average symmetry-protected topological phases](#) (2022), [arXiv:2210.17485 \[cond-mat.str-el\]](#).
- [22] R. Ma, J.-H. Zhang, Z. Bi, M. Cheng, and C. Wang, [Topological phases with average symmetries: the decohered, the disordered, and the intrinsic](#) (2023), [arXiv:2305.16399 \[cond-mat.str-el\]](#).
- [23] T. Rakovszky, S. Gopalakrishnan, and C. von Keyserlingk, [Defining stable phases of open quantum systems](#), *Phys. Rev. X* **14**, 041031 (2024).
- [24] T.-C. Lu, Z. Zhang, S. Vijay, and T. H. Hsieh, [Mixed-state long-range order and criticality from measurement and feedback](#), *PRX Quantum* **4**, 030318 (2023).
- [25] J. Y. Lee, W. Ji, Z. Bi, and M. P. A. Fisher, [Decoding measurement-prepared quantum phases and transitions: from ising model to gauge theory, and beyond](#) (2022), [arXiv:2208.11699 \[cond-mat.str-el\]](#).
- [26] G.-Y. Zhu, N. Tantivasadakarn, A. Vishwanath, S. Trebst, and R. Verresen, [Nishimori's cat: stable long-range entanglement from finite-depth unitaries and weak measurements](#) (2022), [arXiv:2208.11136 \[quant-ph\]](#).
- [27] Y.-H. Chen and T. Grover, [Symmetry-enforced many-body separability transitions](#), *PRX Quantum* **5**, 030310 (2024).
- [28] L. A. Lessa, M. Cheng, and C. Wang, [Mixed-state quantum anomaly and multipartite entanglement](#) (2024), [arXiv:2401.17357 \[cond-mat.str-el\]](#).
- [29] Y.-H. Chen and T. Grover, [Unconventional topological mixed-state transition and critical phase induced by self-dual coherent errors](#) (2024), [arXiv:2403.06553 \[quant-ph\]](#).
- [30] J. Y. Lee, Y.-Z. You, and C. Xu, [Symmetry protected topological phases under decoherence](#), *arXiv preprint arXiv:2210.16323* (2022).
- [31] J. Y. Lee, [Exact calculations of coherent information for toric codes under decoherence: Identifying the fundamental error threshold](#) (2024), [arXiv:2402.16937 \[cond-mat.stat-mech\]](#).
- [32] R. Sohal and A. Prem, [A noisy approach to intrinsically](#)

- mixed-state topological order (2024), [arXiv:2403.13879 \[cond-mat.str-el\]](#).
- [33] T. Ellison and M. Cheng, Towards a classification of mixed-state topological orders in two dimensions, arXiv preprint arXiv:2405.02390 (2024).
- [34] Z. Wang, Z. Wu, and Z. Wang, Intrinsic mixed-state topological order without quantum memory, arXiv preprint arXiv:2307.13758 (2023).
- [35] Z. Wang, X.-D. Dai, H.-R. Wang, and Z. Wang, Topologically ordered steady states in open quantum systems, arXiv preprint arXiv:2306.12482 (2023).
- [36] Z. Wang and L. Li, Anomaly in open quantum systems and its implications on mixed-state quantum phases, arXiv preprint arXiv:2403.14533 (2024).
- [37] H. Xue, J. Y. Lee, and Y. Bao, Tensor network formulation of symmetry protected topological phases in mixed states, arXiv preprint arXiv:2403.17069 (2024).
- [38] Y. Guo, J.-H. Zhang, S. Yang, and Z. Bi, Locally purified density operators for symmetry-protected topological phases in mixed states, arXiv preprint arXiv:2403.16978 (2024).
- [39] R. Ma and A. Turzillo, Symmetry protected topological phases of mixed states in the doubled space, arXiv preprint arXiv:2403.13280 (2024).
- [40] Z. Zhang, U. Agrawal, and S. Vijay, [Quantum communication and mixed-state order in decohered symmetry-protected topological states](#) (2024), [arXiv:2405.05965 \[quant-ph\]](#).
- [41] C. Zhang, Y. Xu, J.-H. Zhang, C. Xu, Z. Bi, and Z.-X. Luo, [Strong-to-weak spontaneous breaking of 1-form symmetry and intrinsically mixed topological order](#) (2024), [arXiv:2409.17530 \[quant-ph\]](#).
- [42] S. Lu, P. Zhu, and Y.-M. Lu, [Bilayer construction for mixed state phenomena with strong, weak symmetries and symmetry breakings](#) (2024), [arXiv:2411.07174 \[cond-mat.str-el\]](#).
- [43] D. Gottesman, [Opportunities and challenges in fault-tolerant quantum computation](#) (2022), [arXiv:2210.15844 \[quant-ph\]](#).
- [44] R. Raussendorf and H. J. Briegel, A one-way quantum computer, *Phys. Rev. Lett.* **86**, 5188 (2001).
- [45] A. Bolt, G. Duclos-Cianci, D. Poulin, and T. Stace, Foliated quantum error-correcting codes, *Physical Review Letters* **117**, [10.1103/physrevlett.117.070501](#) (2016).
- [46] B. J. Brown and S. Roberts, Universal fault-tolerant measurement-based quantum computation, *Physical Review Research* **2**, [10.1103/physrevresearch.2.033305](#) (2020).
- [47] S. Bravyi, M. B. Hastings, and S. Michalakis, Topological quantum order: stability under local perturbations, *Journal of mathematical physics* **51** (2010).
- [48] S. Michalakis and J. P. Zwolak, Stability of frustration-free hamiltonians, *Communications in Mathematical Physics* **322**, 277 (2013).
- [49] S. Sang, L. A. Lessa, R. Mong, T. Grover, C. Wang, and T. H. Hsieh, (in preparation).
- [50] E. Dennis, A. Kitaev, A. Landahl, and J. Preskill, Topological quantum memory, *Journal of Mathematical Physics* **43**, 4452 (2002).
- [51] M. S. Kesselring, J. C. Magdalena de la Fuente, F. Thomsen, J. Eisert, S. D. Bartlett, and B. J. Brown, Anyon condensation and the color code, *PRX Quantum* **5**, [010342](#) (2024).
- [52] S. Paesani and B. J. Brown, High-threshold quantum computing by fusing one-dimensional cluster states, *Phys. Rev. Lett.* **131**, 120603 (2023).
- [53] M. Qi, L. Radzihovsky, and M. Hermele, Fracton phases via exotic higher-form symmetry-breaking, *Annals of Physics* **424**, 168360 (2021).
- [54] S. Roberts and S. D. Bartlett, Symmetry-protected self-correcting quantum memories, *Phys. Rev. X* **10**, 031041 (2020).
- [55] T. Okuda, A. P. Mana, and H. Sukeno, [Anomaly inflow for css and fractonic lattice models and dualities via cluster state measurement](#) (2024), [arXiv:2405.15853 \[quant-ph\]](#).
- [56] G. Q. AI and collaborators, [Quantum error correction below the surface code threshold](#) (2024), [arXiv:2408.13687 \[quant-ph\]](#).
- [57] H. Bombin, D. Litinski, N. Nickerson, F. Pastawski, and S. Roberts, Unifying flavors of fault tolerance with the ZX calculus, *Quantum* **8**, 1379 (2024).
- [58] M. B. Hastings and J. Haah, Dynamically Generated Logical Qubits, *Quantum* **5**, 564 (2021).
- [59] N. Delfosse and A. Paetznick, [Spacetime codes of clifford circuits](#) (2023), [arXiv:2304.05943 \[quant-ph\]](#).
- [60] R. Raussendorf, S. Bravyi, and J. Harrington, Long-range quantum entanglement in noisy cluster states, *Phys. Rev. A* **71**, 062313 (2005).
- [61] W. Brown and D. Poulin, [Quantum markov networks and commuting hamiltonians](#) (2012), [arXiv:1206.0755 \[quant-ph\]](#).
- [62] R. Verresen, U. Borla, A. Vishwanath, S. Moroz, and R. Thorngren, [Higgs condensates are symmetry-protected topological phases: I. discrete symmetries](#) (2024), [arXiv:2211.01376 \[cond-mat.str-el\]](#).